Multi-source remote sensing data analysis for geothermal targeting on Flores island

Christoph Hecker[1], Robert Hewson[1], Agung Setianto[2], Asep Saepuloh[3], Freek D. van der Meer[1]
[1] University of Twente, Faculty ITC, The Netherlands
[2] Universitas Gadja Madah, Yogyakarta, Indonesia
[3] Institut Teknologi Bandung, Bandung, Indonesia
c.a.hecker@utwente.nl; r.d.hewson@utwente.nl; agung.setianto@gmail.com; saepuloh@gc.itb.ac.id; f.d.vandermeer@utwente.nl

Keywords: Flores Island, remote sensing, satellite data, ASTER, SRTM, thermal infrared, lineament-related structure, geothermal

ABSTRACT
Flores Island of Indonesia (Nusa Tenggara Timur) has potential for geothermal energy that is still, for the most part, in its development and exploration phase. There is considerable interest to determine the optimal geothermal exploration techniques and the key area(s) for further investigations on Flores Island. This study summarizes past studies on Flores Island, and the methodology and results of this study's' multi-spectral satellite remote sensing and geospatial techniques used to map geothermal terrain including its fumaroles. In particular, Advanced Spaceborne Thermal Emission and Reflection Radiometer (ASTER) day and night time imagery and Shuttle Radar Topography Mission (SRTM) products were examined to test their suitability for geothermal exploration. However spatial resolution issues as well as vegetation and cloud cover limited the results from day time ASTER image interpretation. The night-time ASTER thermal showed it's potential to identify thermal anomalies associated with volcanic activity on Flores Island however its coarse image pixel size of 90 meters again limited its application. It was found that the SRTM Digital Elevation Model (DEM) as various processed and filtered products, provided a useful geospatial data set to interpret for lineaments that potentially related to the structural features, in part associated with geothermal activity. These preliminary interpreted structural lineament-related structure results were used to recommend areas within the central region of Flores Island to undertake more detailed geothermal investigations at higher spatial resolution using airborne thermal imaging and LiDAR-based DEM techniques.

1 Introduction

The volcanic terrain of Flores Island within the Lesser Sunda Islands of eastern Indonesia is an area highly prospective for geothermal energy. It is located approximately 1500 km east of Jakarta. Interest in its potential has been raised during the collaborative Dutch – Indonesian GEOCAP Project and highlighted during workshop case studies demonstrating remote sensing and geophysical exploration techniques. There are several active geothermal energy fields within its 14250 km2 area however its development is at an earlier stage than other geothermal energy prospects elsewhere in Indonesia such as within Java. Consequently, there is a need to determine the optimal geothermal exploration techniques and key area(s) of interest on Flores Island. This study aims to test optical and thermal multi-spectral remote sensing, and topographic modelling techniques to assist the exploration of geothermal activity on Flores Island. In particular, this study summarises the remote sensing and geospatial interpretation of the imagery derived from the Advanced Spaceborne Thermal Emission and Reflection Radiometer (ASTER) multi-spectral satellite and Shuttle Radar Topography Mission (SRTM). As part of this study, it is also an objective to recommend areas within Flores Island for more detailed geothermal investigations.

The geothermal prospectivity of Flores Island can be divided into three main areas: the Western, the Central (or Bajawa) and the Eastern zones (Figure 1a). These are affected by the various structural tectonic and volcanic features of these regions. Muraoka et al. (2002) describes the large scale subducting and colliding forces from the Australian-Indian, Eurasian and New Guinea plates generating these structural features of Flores Island. In particular, these forces influence the faulting and folding of the Central or Bajawa Zone which in turn also affects the presence of its geothermal fields (Muraoka et al., 2002). Muraoka et al. (2002) highlights and maps these N-S fault lines and the NE-SW to E-W fold axes apparent within the Bajawa Zone (Plate 1, Muraoka et al., 2002). Such faulting and folding also influences the topography, including the volcanic landforms apparent in the Digital Elevation Model (DEM) information derived from the SRTM (https://reverb.echo.nasa.gov/) (Figure 1b). In addition, geothermal and hydrothermal activity can alter the mineralogy of the surrounding host rocks in which the vents or fumaroles release hot chemically enriched fluids. This activity can produce the accumulation of alteration minerals such as various clay, sulphate, opaline-silica and carbonate rich minerals. Characterisation of hydrothermal alteration minerals using shortwave infrared (SWIR) spectroscopy on well drill cores from central Flores Island has previously shown the presence of argillic alteration minerals such as kaolinite, dickite, and halloysite (Aswin and Nanlohy, 2002). This study investigated the feasibility of mapping such alteration indicator minerals using day time ASTER SWIR and thermal infrared (TIR) imagery on Flores Island. Subtle thermal anomalies have also been previously identified using night time ASTER by Urai et al., (2002) in the central Flores Ngada District. Night time ASTER thermal data was examined in this study for signs of temperature anomalies above the surrounding background, suggestive of such surface fumaroles.

Elevation data from the SRTM was also used in this study and interpreted for lineaments and fault lines that could be possibly associated with geothermal fumaroles. It was suggested by Muraoka et al. (2002) that geothermal activity is produced by buried north-south dyke-like magmatic bodies heating fluids that are vented along N-S fractures or

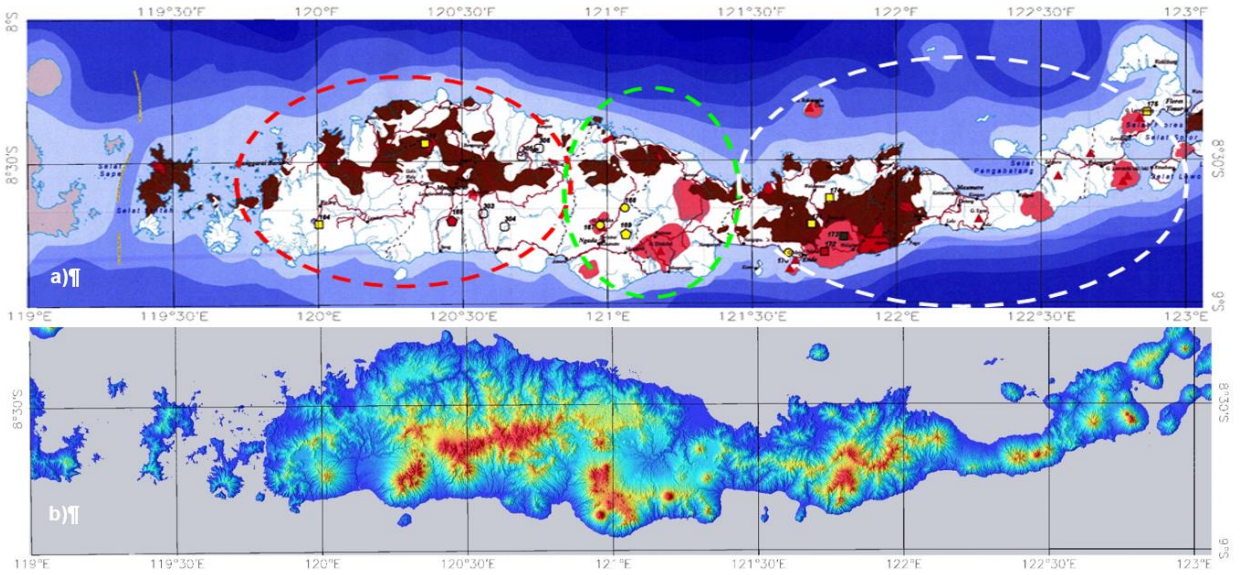

Figure 1:a) Geothermal Prospectivity Map and three significant areas, Western zone(red dashed line), Central (Bajawa) zone (green dashed line) and Eastern zone (white dashed line), supplied by the Indonesian Geological Agency, Bandung; b) SRTM 30m DEM with topogr

faults. Various image processed products from the Digital Elevation Model SRTM data were generated in this study to assist the interpretation of lineaments, including artificially illuminated / shaded relief and slope aspect imagery. Processing and filtering of the Flores Island SRTM DEM by Fourier Filter Transformation (FFT) was also undertaken to assist this interpretation.

The results in this study are presented to show the potential argillic geothermal mineral signatures available in the limited areas exposed to ASTER remote sensing. More significantly, the topographic modelled and filtered DEM products were interpreted for lineaments within the three geothermal Flores Island zones, (Figure 1a) and incorporated into recommendations for future detailed investigations

2 Methodology

2.1 Discriminating geothermal indicator minerals using spectroscopy

The results of fundamental research into mineral spectroscopy (Lyon & Burns, 1963; Adams & Filice, 1967; Hunt & Ashley, 1979; Vincent & Thomson, 1972; Vincent et al., 1975) laid the basis for later geological remote sensing and prompted the launch of such multi-spectral satellite sensors as NASA's Landsat TM in the late 1980s' and ASTER in 1999 by Japan's METI and NASA. The relationship of the spectral bands of Landsat TM, ASTER, HyMap and the more recent WV-3 sensors to common material spectral signatures is shown in Figure 2. The freely available ASTER imagery has the advantage of additional thermal bands, while the new DigitalGlobe commercial WV-3 sensor has higher spatial VNIR-SWIR resolution. ASTER measures six bands within the SWIR wavelength region including the clay / AlOH absorption feature centred at 2.2 um (Figure 3). ASTER bands 5, 6 and 7 have potential to qualitatively reveal changes in the AlOH/clay

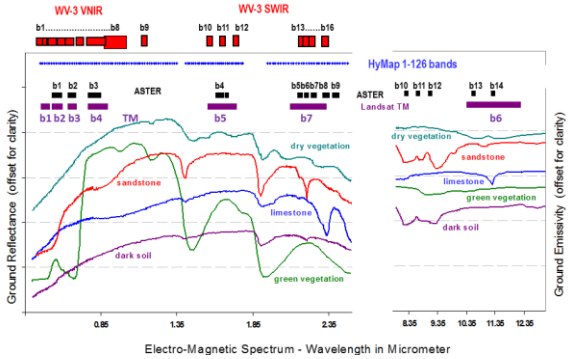

Figure 2:Reflectance spectrum of common surface materials and various remote sensing sensors measuring at these wavelengths

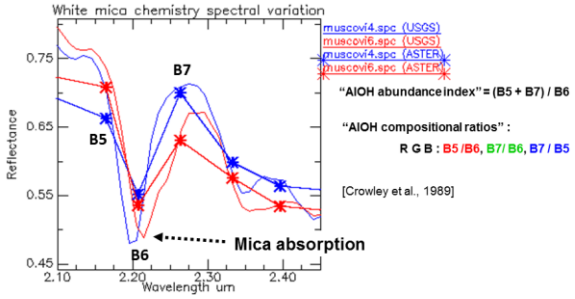

Figure 3: Spectra of AlOH clay/white mica and their ASTER resampled equivalent. Example band parameters as listed, estimate AlOH clay content and composition

composition from changes in the absorption feature wavelength shift (Figure 3). Abundance and compositional indices for minerals and/or mineral groups with absorption features such as AlOH in Figure 3, can be devised as shown using such band ratios and relative band depth arithmetic

(Crowley et al., 1989). Table 1 summarises some of the key geothermal minerals described by Brady et al. (2006) and Littlefield & Calvin (2014). Each potential indicator mineral is listed with potentially diagnostic band ratio / relative band depth algorithms, as calculated from spectral data from the described wavelength regions (Table 1).

Table 1: Key geothermal minerals and their representation with ASTER band parameters derived from the listed wavelength regions

Indicator Geothermal minerals	Potential diagnostic wavelength region	ASTER band parameter
Quartz ; Opaline silica	TIR ; SWIR	B13 / B10 ; (B5 + B8) / (B6 + B7)
Alunite	SWIR	B7 / B5
Kaolinite	SWIR	B7 / B5
Montmorillonite	SWIR	(B5 + B7) / B6
Chlorite	SWIR	(B6 + B9) / (B7 + B8) ; (or (B6 + B9) / B8) ; (Masked by higher values B5 / B4 Ferrous)
Calcite	SWIR; TIR	(B6 + B9) / (B7 + B8) ; (or (B6 + B9) / B8) ; B13 / B14
Gypsum	TIR	(B10 + B12) / B11

Example spectral signatures of these indicator minerals from the USGS VNIR-SWIR spectral library (Baldridge et al. 2009) as laboratory and at equivalent ASTER band resolution are shown in Figures 4. Similarly TIR signatures for some geothermal indicator minerals are shown using the Johns Hopkins University spectral library (Baldridge et al. 2009) and for their equivalent ASTER band resolution in Figure 5.

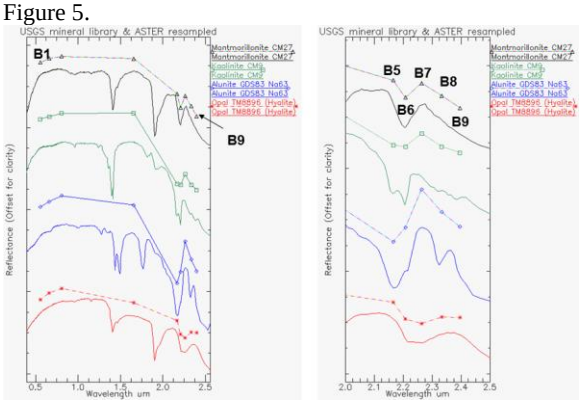

Figure 4: a) Spectra of montmorillonite, kaolinite, alunite and opaline silica and their ASTER resampled equivalent 0.5 to 2.5 um; b) Close up of spectra 2.0 to 2.5 um

2.2 Extracting lineaments from topographic modelled and filtered DEMs

DEMs derived from SRTM is available at 30 metre pixel resolution from the NASA/USGS REVERB data portal (https://reverb.echo.nasa.gov/). Several versions of the SRTM DEM data are available including the 90 metre and the recently released 30 metre resolution versions (https://lta.cr.usgs.gov/SRTM1Arc). This study accessed and utilised the SRTM 1 Arc-Second Global data at 30 m resolution in GeoTIFF format and mosaicked the downloaded 1 degree tiles encompassing the Flores Island.

Topographic modelling of the SRTM DEM imagery was undertaken using ENVI version 5.3 software (http://www.harrisgeospatial.com/ProductsandSolutions/GeospatialProducts/ENVI.aspx) to generate shaded relief and aspect image products. Shaded relief was simulated at different illuminated azimuth (0 and 270 degrees) and elevation angles (50-60 degrees) to enhance the N-S and ENE-WSW to E-W fault lines and fold axes described by Muraoka et al. (2002). The aspect slope imagery was classified into 4 classes, NNE (45-90o), SSE (135-180o), WSW (225-270o) and NNW (315-360o).

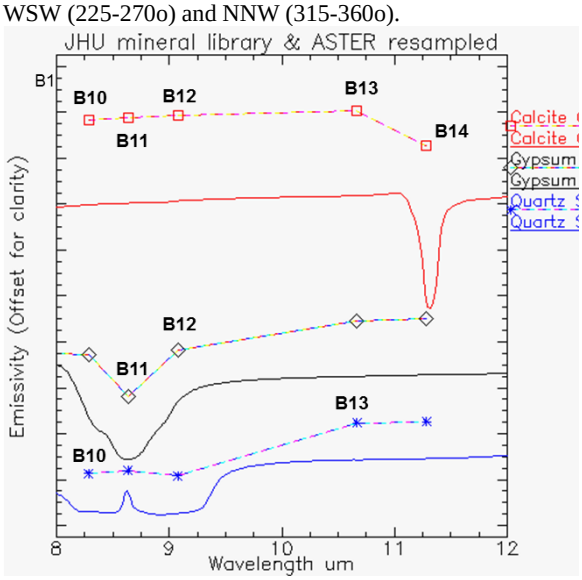

Figure 5: Spectra of calcite, gypsum and quartz within the thermal wavelengths 8 to 12 um

FFT filtering of the Flores island DEM imagery was undertaken using techniques described by Florinsky (2012) and using the ENVI version 5.3 software (http://www.harrisgeospatial.com/ProductsandSolutions/GeospatialProducts/ENVI.aspx). Two FFT filtered versions of the SRTM data were generated to enhance the higher spatial frequency DEM information. User defined elliptical high pass cut off filters were applied, with a border margin of 50 pixels to reduce high frequency artefacts at the filter margins, before an inverse FFT was applied to generate the filtered DEMs (Figure 6 a, b & c).

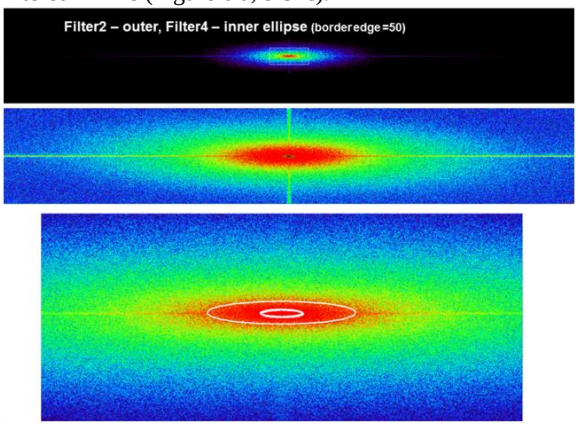

Figure 6: Images representing 2 D FFT spectrum of SRTM 30 m DEM a) complete 2D spectrum; b) close up of a); c) close of b) showing the cutoff filters applied and shown in Figure 13 e.g. Filter 2 = outer ellipse, Filter 4 = inner ellipse

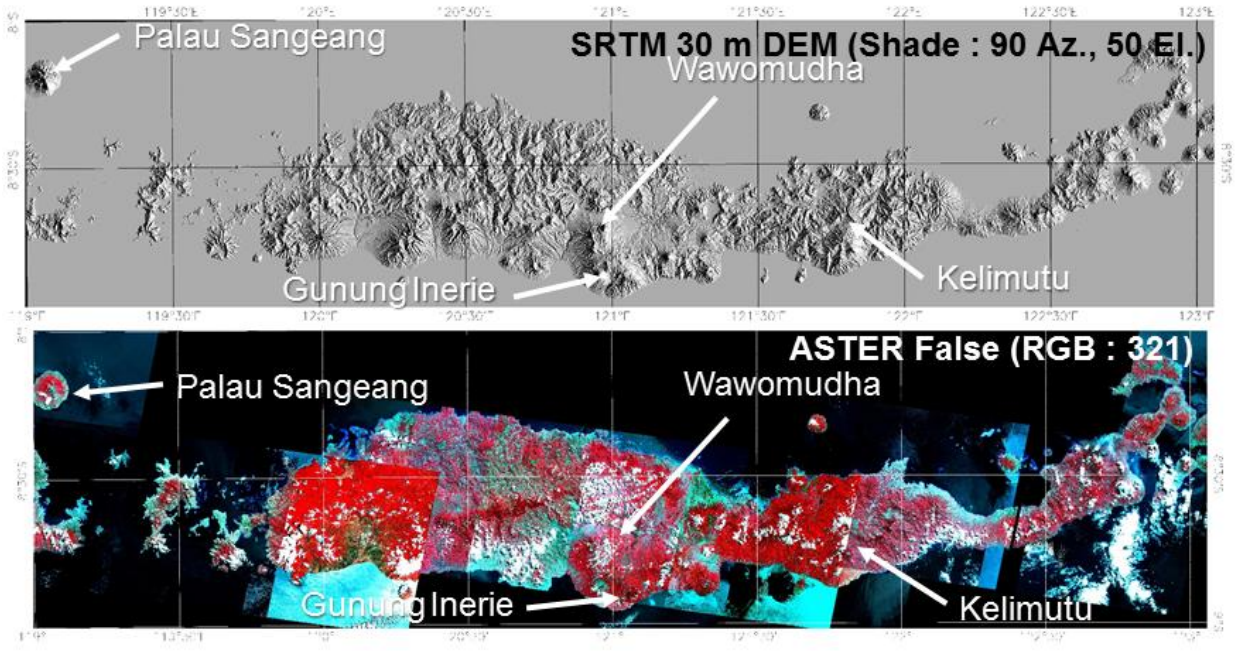

Figure 7: a) SRTM 30m DEM with topographic shading from easterly illumination; b) ASTER false colour (RGB : Bands 3,2,1). Sites of major volcanos with bare exposures are listed

These FFT filtered products were generated in an attempt to separate large scale volcanic topography (e.g. cones) from the more subtle and higher spatial frequency ridges and land forms, potentially related to fracture lineaments. ERDAS ERMapper software (http://www.hexagongeospatial.com/products) was also used for the final display and lineament interpretation of the above DEM products for each of Western, Central and Eastern Flores Island geothermal zones (1a).

3 Results

3.1 ASTER map products and spectral signatures in exposed Flores Island sites

The densely vegetated and often cloud covered mountainous terrain in Flores Island proved a challenging area to use ASTER imagery (Figure 7a and b). The False colour RGB composite of ASTER bands 3, 2 and 1 highlights the chlorophyll vegetation in areas of bright red in this multiple ASTER scene mosaic that covers Flores Island (Figure 7b). Several sites (Figure 7a and b) were examined in this preliminary study as part of the Advanced Geothermal Exploration Workshop, Bandung, 2016.

Mt Inerie in Central Flores is a prominent volcanic landform with some large exposed bare rock surfaces on its slopes. The ASTER VNIR False colour and Normalised Difference Vegetation Index (NDVI) imagery showed no or reduced green vegetation on Mt Ineries' slopes, particularly on its northern and northeastern flanks (Figure 8a and b). Kaolinite and AlOH clay is detected by the ASTER band products in its northern slopes (Figure 8c). The south eastern flanks are affected by thick cloud cover. However, problems with cloud artefacts are apparent in the southern slopes (Figure 8c). A preliminary examination of the ASTER VNIR-SWIR surface reflectance spectra within

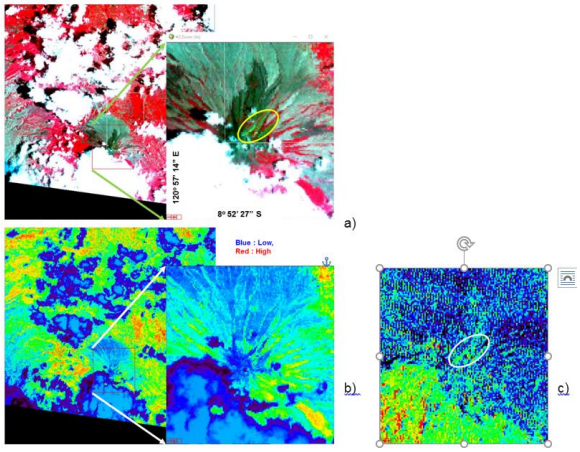

Figure 8: Inerie volcano and associated ASTER products: a) ASTER false colour (RGB : Bands 3,2,1); b) NDVI (low vegetation: blue; high : red); c) Kaolinite content (blue : low; red : high). Circled area shows clay

Ineries' exposed slopes reveal argillic / clay and possibly MgOH/carbonate signatures.

The Wawamudha volcano, also in central Flores, contained another limited exposed area of bare rock ground to apply ASTER's remote sensing. This area also revealed possibly argillic altered clay spectral signatures (alunite?) although further validation ground/field truthing is required.

3.2 Mapping thermal anomalies using ASTER surface kinetic temperature products

The volcanic activity at Palau Sangeang (Figures 7 a & b, 9), just offshore the north western coast of Flores Island, offers the opportunity to test the mineral mapping and

thermal anomaly mapping capabilities of ASTER imagery. The issue of cloud and vegetation cover also proved a difficulty here but two scene acquisitions (2004-11-04 and 2006-09-07) were merged to reduce at least the effects of the clouds (Figure 9). The two options of image merging were interpreted for AlOH / clay content with mixed results. The ASTER scene acquired on 2006-09-07, and to a lesser extent the 2004-11-04 acquisition, revealed clay anomalies particularly in the central part of the island (Figure 10). The surface kinetic temperature products generated from these two day-time ASTER acquisitions revealed variable temperature anomalies, with a noticeable anomaly of 53o C at the summit of the volcanic dome for the 2006-09-07 scene (Figure 11).

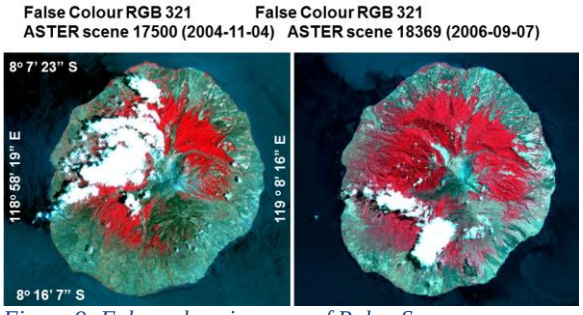

Figure 9: False colour imagery of Palau Sangeang

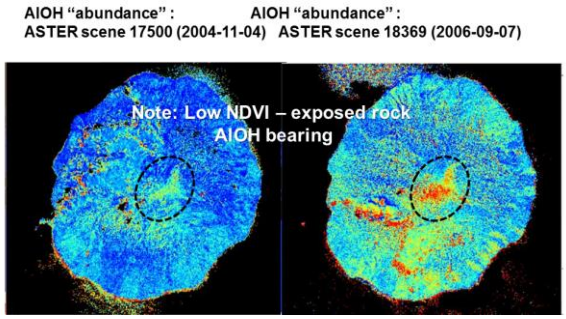

Figure 10: ASTER AlOH content interpretation of Palau Sangeang. Black dashed circle area highlights exposed potential clay altered areas (green to red). Note cloud shadow artefacts producing false anomalies south west of ASTER scene 18369 (right).

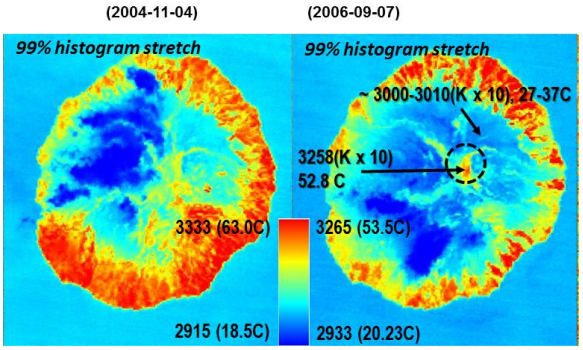

Figure 11: Day time ASTER surface kinetic temperature product of Palau Sangeang. Black dashed circle area highlights bare exposed area described in Figure 16

Surface kinetic temperature products from night time ASTER acquisitions over Palau Sangeang were accessed from seven dates between 2003-05-12 to 2014-08-21 and shown as an overlay to shaded DEM relief in Figure 12. These generally highlighted the cooling effect of the elevated volcanic summit at night however anomalously higher temperatures were observed from 2014-06-02 to 2014-08-21. In particular a river of hot lava appears apparent running down its flanks on the 2014-07-20 and 2014-08-21. However night time ASTER thermal imagery accessed and examined over the rest of Flores Island failed to identify isolated anomalies, potentially associated with geothermal fumaroles. There were less night time than the day time acquisitions available which may handicap their recognition, depending on the geothermal activity duration. However the night time ASTER temperature data over the Mt Inerie area did reveal a similar subtle thermal anomaly, as described by Urai et al., (2002) (Urai et al.,'s Figure 8). Urai et al., (2002) found a rise in the ASTER brightness temperature anomaly approximately 6 km east of Mt Inerie, in the Nage geothermal area. As with Urai et al. (2002)'s study, a subtle anomaly of only a few degrees above background temperature was observed. It should be noted that any thermal anomaly would be an averaged estimate over the measured 90 metre ASTER TIR pixels.

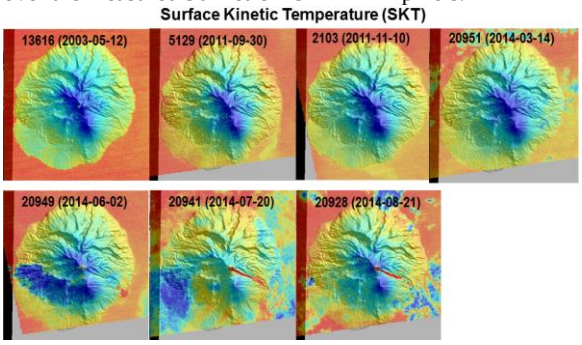

Figure 12: Chronological sequence of night time ASTER surface kinetic temperature imagery of Palau Sangeang draped over SRTM 30m DEM. Blue : low temperature; red high. Note high temperatures associated with lava flows from 2014-06-02 to 2014-08-21.

3.3 Lineament interpretation from SRTM DEM products

Examples of the products generated from the SRTM DEM for structural interpretation are shown in Figure 13 for an area in the Central Zone. The high quality SRTM DEM at 30 metre pixel resolution is apparent from the elevation display and shaded relief product in the central geothermal zone (Figures 13 a & b). The FFT filtered DEM products derived from the high pass cutoff filters 4 (moderate frequency pass filter) and 2 (high pass frequency filter) shown in Figure 6, are indicated for this same area in Figures 13 c and d, respectively. The north – south topographic features are generally more apparent in the moderate high pass frequency product (Figure 13 c) with only the more subtle finer features shown in the higher pass filtered product (Figure 13 d). Figures 14 a to d show an example from the Flores Bajawa area, include the locations of the established geothermal fields, lineament interpretation from the area. The lineaments shown are a

compilation of the interpretation from the various DEM map products described in Section 2.2 and 3.2.

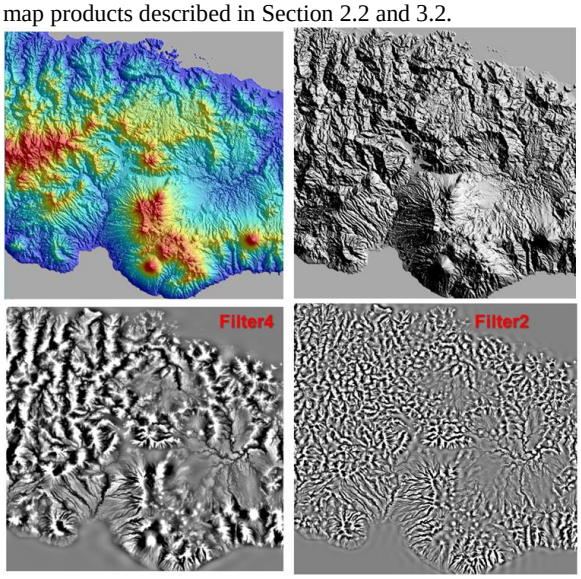

Figure 13: Example imagery of Central Flores SRTM 30 m imagery. a) Pseudo coloured DEM draped over sun shaded imagery; b) Sun shaded imagery (azimuth : 90 degrees, elevation 55 degrees; c) FFT 2-D filtered at moderate pass spatial frequency (Filter4); d) FFT 2-D

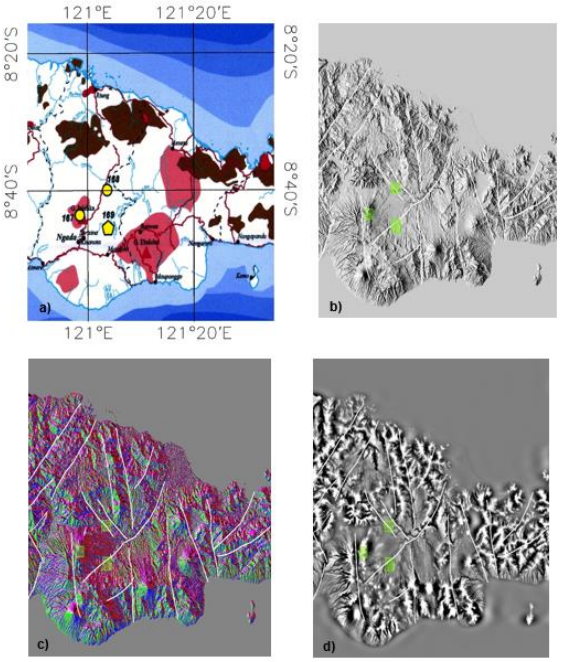

Figure 14: a) Central zone of Flores Island, supplied by the Indonesian Geological Agency, Bandung; b) Shaded DEM with lineament interpretations; c) Aspect modelled from DEM with lineament interpretations; d) FFT 2-D filtered at moderate high pass spatial frequency (Filter4) with lineament interpretations. Geothermal fields shown as green squares

4 Conclusion and recommendation

Vegetation and cloud cover on Flores Island together with ASTER's coarse 30 metre SWIR pixel resolution combine to limit the application of day time ASTER VNIR-SWIR remote sensing for the mapping geothermal indicator minerals. Spectral signatures from small exposures within volcanic terrain do suggest the presence of argillic minerals however ground truthing and spectroscopy of field samples is required. If future field sampling and spectrometer measurements prove successful in identifying geochemical indicator minerals then field or laboratory proximal sensing could be useful as a routine and efficient technique for ground based geological and geothermal prospect mapping.

The application of ASTER night-time thermal imagery also provided limited results for geothermal anomalies mainly because of the coarse spatial resolution of the ASTER TIR instrument (e.g. 90 metre pixels). Averaging temperature anomalies from geothermal fumaroles of a few metres in dimension, from a 90 x 90 metre pixel sampling area will limit the chances of their discovery. It is anticipated however that a higher spatial resolution thermal sensor or camera, capable of measuring radiance or surface temperature of within smaller pixel dimensions could prove more successful at detecting active geothermal fumaroles.

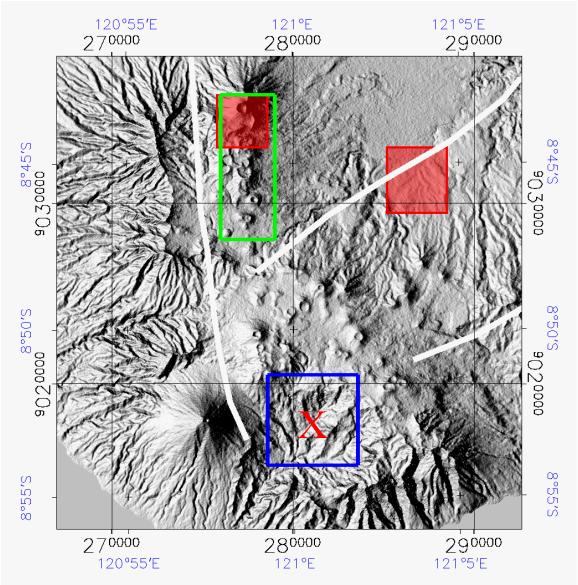

Figure 15: Shaded SRTM DEM within the Central Bajawa Zone of Flores Island, showing recommended detailed study areas A (blue box) and B (green box) for further high spatial resolution Lidar DEM and thermal imaging. Red X : Nage geothermal area (Urai et al., 2002)

The lineament interpretation from the SRTM DEM products are likely to include geomorphological features that may or may not be related to fault lines or fractures associated with geothermal activity. The trends of these lineaments however appear generally consistent with the NNW and NE trends of fault structures and fold axes described by Muraoka et al. (2002). The lineaments interpreted for the Central or Bajawa Zone (Figure 14 b, c & d) show a relatively high density and pass through the

currently recognized geothermal fields as marked. This area is also in the vicinity of the Nage geothermal area east of Mt Inerie, previously identified by thermal imagery (Urai et al., 2002). This suggests that this is an area worthy of further investigations for more detailed structural studies and thermal observations. The shaded relief DEM product also reveals the presence of minor cones in a north-south alignment north of Mt Inerie, as shown in Figure 14 b, and at a finer scale in Figure 15. Two areas are recommended to undertake more detailed LiDAR DEM and thermal camera observations, areas A (25 km2) and B (24 km2) as marked in Figure 15. Higher resolution LiDAR deployed in a ground return mode, should facilitate more detailed structural features such as fractures and fault lines. Also airborne thermal camera with a higher spatial resolution also offers the potential to detect the hydrothermal emissions from fumaroles of limited dimensions.

5 Acknowledgements

This study was financially supported by the Geothermal Capacity Development Programme Indonesia-Netherlands (GEOCAP). The ASTER L2 data products were retrieved from the online Data Pool, courtesy of the NASA Land Processes Distributed Active Archive Center (LP DAAC), USGS/Earth Resources Observation and Science (EROS) Center, Sioux Falls, South Dakota, https://lpdaac.usgs.gov/data_access/data_pool. The authors would also like to thank the Indonesian Geological Agency, Bandung for supplying a hardcopy map of the geothermal potential areas of Nusa Tenggara Timur.

6 References

Adams J.B. and Filice, A.L., (1967). "Spectral reflectance 0.4 to 2.0 microns of silicate rock powders", *Journal of Geophysical Research*, 72, pp. 5705–5715.

Aswin, D and Nanlohy, (2002), "Characteristic of hydrothermal alteration minerals on MT-1 and MT-2 wells, Mataloko, central Flores, East Nusatenggara, Indonesia by using short-wave infrared reflectance spectroscopy", *Bulletin of Geol. Surv. Japan*, vol. 53, pp. 323-328.

Baldridge, A. M., S.J. Hook, C.I. Grove and G. Rivera, 2009. "The ASTER Spectral Library Version 2.0," *Remote Sensing of Environment*, vol 113, pp. 711-715.

Crowley, J.K., Brickley, D.W. and Rowan, L.C. (1989), "Airborne imaging spectrometer data of the Ruby Mountains, Montana: mineral discrimination using relative absorption band-depth images", *Remote Sensing of Environment*, 29, pp. 121–134.

Florinsky, I.V. (2012), "Digital Terrain Analysis in soil science and geology", Elservier, Amsterdam, First Ed., 2012, ISBN 978-0-12-385036-2

Hunt, G.R. and Ashley, R.P. (1979), "Spectra of altered rocks in the visible and near infrared", *Economic Geology*, v. 74, pp. 1613–1629.

Kratt, C., Calvin, W., and Coolbaugh, M., (2006), "Geothermal exploration with Hymap hyperspectral data at Brady–Desert Peak, Nevada*", Remote Sensing Environ*., Vol. 104, pp. 313-324.

Littlefield, E.F. and Calvin, W.M., (2014), "Geothermal exploration using imaging spectrometer data over Fish Lake Valley, Nevada", *Remote Sensing Environ*., Vol. 140, pp. 509-518.

Lyon, R.J.P., and Burns, E.A. (1963), "Analysis of rocks and minerals by reflected infrared radiation*", Economic Geology*, 58, pp274–284.

Muraoka, H., Nasution, A., Urai, M., Takahashi, M., Takashima, I., Simanjuntak, J., Sundhoro, H., Aswin, D., Nanlohy, F, Sitorus, K., Takahashi, H., and Koseki, T., (2002), "Tectonic, volcanic and stratigraphic geology of the Bajawa geothermal field, central Flores, Indonesia," *Bulletin of Geol. Surv. Japan*, vol. 53, pp.109-138.

Urai, M., Muraoka, H., and Nasution, A., (2002), "Satellite remote sensing data and their interpretations for geothermal application: A case study on the Ngada District, central Flores, Indonesia.", *Bulletin of Geol. Surv. Japan*, vol. 53, pp. 99-108.

Vincent, R.K. and Thomson, F. (1972), "Spectral compositional imaging of silicate rocks," *Journal of Geophysical Research*, 77, 14, pp2465–2472.

Vincent, R.K, Rowan, L.C., Gillespie, R.E. and Knapp, C., (1975), "Thermal-infrared spectra and chemical analyses of twenty-six igneous rock samples", *Remote Sensing of Environment*, 4: 199-209. International Geoscience and Remote Sensing Symposium (IGARSS), 9–13 July. 3p.